ABSTRACT

LEDFORD, JOHN CHRISTOPHER. Synthesis and Properties of Binary and Ternary Iron Based Superconductors via Mechanical Alloying. (Under the direction of Dr. Frank Hunte).

With the emergence of the iron-based superconductors, research efforts have been focused on the processing routes necessary for the synthesis of pure samples (free of extra phases) which exhibit strong superconducting properties. In this work, iron selenide ($Fe_{1.015}Se$) was prepared using planetary ball milling for 48 hours and pressed into pellets with subsequent heat treatment at 400 °C for 24 hours. The pellets were annealed inside a tungsten carbide die to minimize loss of selenium during heat treatment. The composition and confinement during annealing allowed for the synthesis of high purity samples with approximately 94% of the superconducting β-FeSe phase as determined by Rietveld analysis of the XRD data. The temperature of the onset of the superconducting transition (T_c) was 9.0 K at 90% ρ as determined by transport measurements with a zero resistivity temperature of 7.8 K. This transition width is narrow compared to other reported samples of similar processing and is attributed to the high percentage of β-FeSe present in the sample. Magnetization measurements yielded a transition temperature of 8.0 K which is in agreement with the T_c obtained from transport measurements. The upper critical field ($H_{c2}(0)$) of this sample was 27.5 T determined at 90% ρ and using a Werthamer–Helfand–Hohenberg (WHH) fit to the data. This high $H_{c2}(0)$ for the polycrystalline samples is comparable to that reported for single crystal samples.

Our follow up work focused on the ternary, $Fe_{50}Se_{25}Te_{25}$, which was synthesized utilizing planetary ball milling, high energy SPEX milling, and cryomilling. $Fe_{50}Se_{25}Te_{25}$ was either planetary ball milled for 48 hours, high energy SPEX milled for 20 hours, or cryomilled

for 4 hours. All powders were pressed into pellets with subsequent heat treatment at 700 °C for 1 hour and 700 °C for 40 hours. The superconducting temperature for the high energy SPEX milling and cryomilling was shown to be the highest of the three milling processes with a temperature around ~14.3K. The upper critical field ($H_{c2}(0)$) was found to be highest in the high energy ball milling processes most likely due to a higher concentration of defects introduced during the milling process. Magnetization measurements are in agreement with the T_c obtained from transport measurements. The planetary ball milling and cryomilling magnetization measurements showed a transition around ~120K which has shown to be a phase transition but disappears in the high energy SPEX milling. The critical current measurements showed the highest value of 935 mA for the planetary ball milling process with the high energy SPEX milling falling shortly behind. Critical current for the cryomilled samples showed a drastic decrease by almost half.

Synthesis and Properties of Binary and Ternary Iron Based Superconductors via Mechanical Alloying

by
John Christopher Ledford

A thesis submitted to the Graduate Faculty of
North Carolina State University
in partial fulfillment of the
requirements for the degree of
Master of Science

Materials Science and Engineering

Raleigh, North Carolina

2015

APPROVED BY:

_____	_____
Dr. Frank Hunte Committee Chair	Dr. C. Lewis Reynolds Jr.
_____	_____
Dr. Ronald Scattergood	Dr. Carl Koch

DEDICATION

I would like to dedicate this work to my family and friends for their tireless support throughout my academic career

BIOGRAPHY

John Christopher Ledford was born in Lincolnton, NC and raised there his entire life. He attended Lincolnton High School and graduated in the spring of 2009. During his high school career, he attended several engineering based summer camps and that is how he decided to pursue a degree in Materials Science and Engineering. He received his bachelor of science in Materials Science and Engineering at North Carolina State University in the spring of 2013.

ACKNOWLEDGMENTS

I would like to thank my committee members; Dr. Hunte, Dr. Reynolds, Dr. Scattergood, and Dr. Koch for all of their help with my research and assistance through graduate school. I would like to thank Dr. Zhu for the use of his glovebox which allowed me to continue with my project. I would like to thank my fellow group members, Christer and Raj, for all their help in getting me to this point in my career. There was never a moment when they would not lend a helping hand and I am grateful for that. I would like to thank Edna for all of her help through the process and making sure that everything was taken care of.

A special thanks to Roger and Toby for all the help over the years in not only school and research but so much more in my personal life. I have a countless number of friends which I have to thank for all their help with school, research, and life in general and would like to extend my gratitude to everyone who has helped me along the way.

I would like to my family for their tireless support through the years and their encouraging words when things did not always go as planned. I would like to thank for Rachel for her tireless support over the past few months and motivation to get it all done.

TABLE OF CONTENTS

LIST OF TABLES

LIST OF FIGURES

Chapter 1

Introduction

Superconductivity has been the subject of extensive research since its discovery in 1911 by Dutch physicist Heike Kamerlingh Onnes. Onnes was the first scientist to liquefy helium which allowed him to make the first observations of superconductivity as the electrical resistance of pure mercury dropped to zero below its critical temperature $T_c \sim 4.2K$ [1, 2]. Following this observation, low temperature resistivity measurements were performed on a number of pure elements and alloys to determine what other materials might show this newly discovered phenomenon which Onnes called superconductivity.

A significant characteristic of superconductivity is the observation of zero resistivity below some critical temperature as compared to normal metals which retain some residual resistivity down to the lowest temperature. The resistivity of a superconducting material in the normal state is comparable to or higher that of a typical metal.

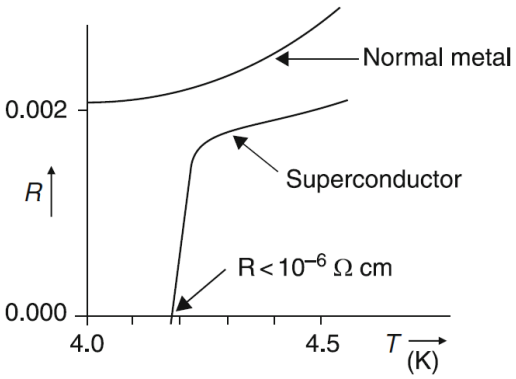

Figure 3.1: Temperature dependence of resistance of a normal metal and a superconductor [3]

The existence of the superconducting state is dependent on the temperature at which the superconductor is maintained, the magnetic field which is present and current which it conducts. Superconductors are classified into two categories, type I & II, which describes their behavior when an external magnetic field is applied. Type I superconductors show a sharp transition from the superconducting state to the normal state when a sufficiently high magnetic field is applied. Type I superconductors are typically pure metals. Type II superconductors exhibit a different behavior and are characterized by two critical fields, the upper and lower critical fields. Below the lower critical field, H_{c1}, the externally applied magnetic field is completely expelled from the interior of the superconductor. Above the upper critical field, H_{c2}, the externally applied magnetic field penetrates the superconductor causing it to revert to the normal state. A mixed state exists between the lower critical and upper critical fields where the material maintains superconducting properties with the existence of a flux vortex lattice. Applied currents in the superconductor can also cause superconductivity to diminish and/or disappear. This critical current density, J_C, is the maximum amount of lossless current that the superconductor can support before superconductivity breaks down and a voltage is observed. This occurs because the overall magnetic field in the superconductor exceeds the critical field value due to the transport current and externally applied magnetic field [3].

High temperature superconductors were first discovered in 1986 by Bednorz and Müller when they observed superconductivity in the Ba-La-Cu-O system with a critical temperature of ~35K in $La_{2-x}Ba_xCuO_4$ [4]. These are oxide based superconductors and often referred to as the cuprate materials due to the Cu-O layers present in the material. Soon after this discovery of the cuprates, Chu discovered that $LnBa_2Cu_3O_{7-\delta}$ (Ln = Y, Nd, Sm, Eu, Gd,

Dy, Ho, Er, Tm, Yb),also called the 123 oxides, showed superconductivity in the 90K range which is higher than the boiling point of nitrogen [5]. With transition temperatures climbing higher and higher, the race to discover a room temperature superconductor has fueled recent research in the field.

Iron-based superconductors have been extensively researched since the discovery of $La[O_{1-x}F_x]FeAs$ in 2008 [6]. Prior to this discovery, it was thought that the presence of a ferromagnetic element such as iron in a material would be detrimental to the superconducting state. This prolific research effort worldwide has to date revealed six families of materials that are classified by structure as 11, 111, 1111, 122, 32522, and 42622 compounds including both pnictides and chalcogenides [7]. These classes are representative of the chemical makeup of the compounds such as the 11 class representing FeSe. The pnictides include compounds from group 15 elements such as arsenic (As) and phosphorus (P). The chalcogenides include compounds from group 16 elements such as sulfur (S), selenium (Se), and tellurium (Te). Of these novel superconductors, $Sm[O_{1-x}F_x]FeAs$ was found to have the highest transition temperature of 55 K while many of the materials showed very high upper critical fields which could potentially be useful for high magnetic field applications [8, 9]. These materials have an intriguing and varied chemistry and display many interesting manifestations of unconventional multiband superconductivity and the interplay of magnetism and superconductivity. A drawback to the study of the iron-based families of superconductors is the incorporation of arsenic which is toxic and can be highly reactive under certain processing conditions when moisture is present. In order for these compounds to be investigated for use in commercial applications, it would be advantageous if these potentially hazardous additions

could be substituted by safer materials. It has been shown that iron chalcogenides can show superconducting behavior while not containing these toxic additions such as the pnictides.

FeSe is structurally the most simple of the iron-based superconducting materials with a tetragonal superconducting phase in which superconductivity has been observed so far with a T_c ~8 K [7, 10]. Medvedev *et al* used pressures up to 9GPa to increase the transition temperature to 36.7K [11]. McQueen *et al* found that the stoichiometry for the β-FeSe superconducting phase is extremely sensitive to changes in the selenium content. A slightly non-stoichiometric composition in favor of iron is needed in order to produce a pure superconducting sample. When the stoichiometry of the samples is iron-rich then the β-FeSe is formed along with excess iron. When the stoichiometry is not iron-rich, then the β-FeSe is formed along with the δ-FeSe phase which is not superconducting. A temperature range also exists between 300 and 450K for which a pure β-FeSe phase is possible and below this range the hexagonal FeSe phase is dominant [12]. It has been shown that tellurium substitution of the binary FeSe compound can increase the transition to ~15K and is not nearly as stoichiometrically sensitive as FeSe. The optimal substitution level of tellurium seems to be around 50% but can vary and still show a superconducting phase [13-15].

Sefat discusses the processing techniques that are most commonly used to produce these iron based superconductors which are the solid state method, Bridgman method, and the flux method [16]. The solid state method uses powders which are mixed in the correct atomic ratios of the compound being formed and are heated for extended periods of time at elevated temperatures. These reactions are carried out in sealed containers to prevent contamination and loss of material during heating. The process relies on diffusion of ions instead of melting

to form the new compounds [16]. This can lead to a long sample preparation time in order to get a truly uniform sample and in most cases the samples will be small in size. The Bridgman method melts the chemical elements of the compound to be produced and then slowly cooled to allow crystallization of the superconducting phase. This process is done in an inert crucible which has been sealed to prevent loss of any precursors. Care must be taken in the synthesis of some compounds due the high melting temperatures of the precursors and synthesis vessel thermal stability. The flux method uses a supersaturated solution which is slowly cooled to allow crystallization of the superconducting phase similar to that of the Bridgman method. This method allows for shorter crystal growth times and lower temperature synthesis [16]. Both the Bridgman and flux methods produce small single crystal samples. Another processing technique that can be implemented in the synthesis of these iron based superconductors is mechanical alloying also known as ball milling.

Few studies have investigated the mechanical alloying process in the production of these iron chalcogenides. Xia *et al* were first to synthesize the superconducting β-FeSe via the mechanical alloying process [17]. A high energy milling process was utilized which resulted in nanoscale precursors, which helped to facilitate the formation of the superconducting phase during the annealing process. It was found that longer milling times resulted in the formation of δ-FeSe which is the non-superconducting phase. By annealing the samples at 400°C, the superconducting β-FeSe showed a transition of ~8.9K when the samples were selenium deficient [17]. Li has also looked into the synthesis of FeSe via the ball milling process but instead of used a lower energy technique known as planetary ball milling to synthesize samples. It was shown that a longer milling time resulted in a higher percentage of the β-FeSe

superconducting phase due to the formation of $FeSe_2$ which resulted in a reduction of evaporation of selenium giving a more favorable stoichiometry. It was also shown that with an extended milling time (>50 hours) that the superconducting phase was suppressed as seen by Xia [18]. Li however shows that a higher sintering temperature of 750°C produces a higher percentage of the β-FeSe phase which produced a transition temperature of ~10.1K measured by resistance [19]. Li also reported planetary ball milling of the ternary Fe-Se-Te which has a higher transition temperature. It was found that also with shorter milling times the amount of β-FeSe superconducting phase increased which helps to enhance the overall superconducting properties. The 20 hour ball milled sample showed a transition temperature of ~14K while the 80 hour milled sample showed no superconducting properties [20].

The purpose of this research was to investigate the effects that the mechanical alloying process has on the superconducting properties of these iron based superconductors. The binary FeSe was chosen because it is chemically the most simple of the iron based superconductors and a model system to study the effects that a mechanical alloying process would have on the superconducting transition temperature also in addition the upper critical field for these iron-based superconductors. FeSeTe was chosen due to its higher superconducting transition temperature but still being one of the simple iron based superconductors. Another factor for choosing these alloys was the elimination of the arsenic which is prevalent in many of the other iron based compounds and instead utilizing selenium and tellurium which are much safer to work with. We hypothesize that the mechanical alloying process will allow for a simplified route to bulk synthesis for these iron based superconductors while enhancing the superconducting properties such as the transition temperature and upper critical field. The

enhanced superconducting properties will be a direct result from the milling process due to the high alloying ability of the process which will result in a higher superconducting phase percentage when coupled with the correct sintering procedure.

Chapter 2

Synthesis of FeSe and FeSeTe

$Fe_{1.015}Se$ and $Fe_{50}Se_{25}Te_{25}$ samples were prepared using pure Fe, Se, and Te powders (Alfa Aesar/99.9%/200 mesh, Alfa Aesar/99.999%/<10 micron, and Alfa Aesar/99.99%/200 mesh respectively). The powders were loaded into a stainless steel vial under an argon atmosphere and sealed with an O-ring as seen in Figure 2.1.

Figure 4.1: Stainless steel vial and milling media used for $Fe_{50}Se_{25}Te_{25}$ synthesis

Stainless steel milling balls (6.35 mm and 7.94 mm diameters) were used in a 10.2:1 ball to powder ratio. In order to alloy the powders, a combination of three different ball milling techniques was utilized to prepare compacted disc samples for characterization. Initially,

powders were planetary ball milled at 275 rpm using a GlenMills Planetary Ball Mill for 48 hours as seen in Figure 2.2.

Figure 2.2: Planetary ball mill setup for $Fe_{50}Se_{25}Te_{25}$ synthesis

This milling process was chosen because it is a lower energy process and contamination from the milling vial and media could be minimized. Powders were milled using a SPEX 8000 high energy ball mill for 24 hours at room temperature as seen in Figure 2.3.

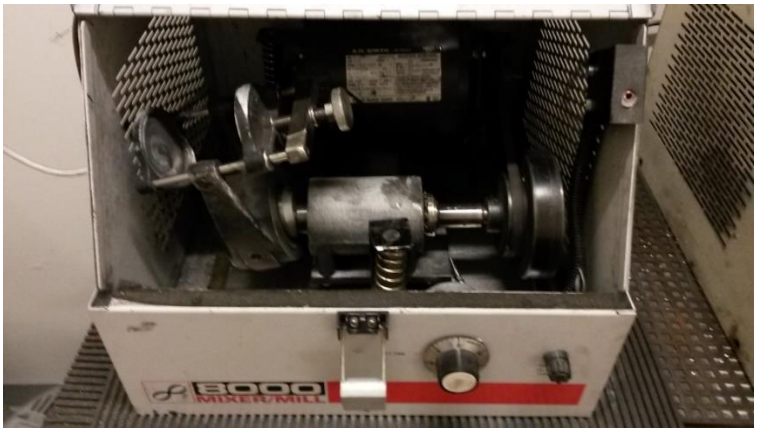

Figure 2.3: High energy SPEX ball mill setup for $Fe_{50}Se_{25}Te_{25}$ synthesis

Powders were cryomilled utilizing a liquid nitrogen cooled SPEX 8000 high energy ball mill for 4 hours. The vial was cooled down initially by submerging in liquid nitrogen and then transferring to the mill where liquid nitrogen flowed through a nylon jacket during the milling process as seen in Figure 2.4.

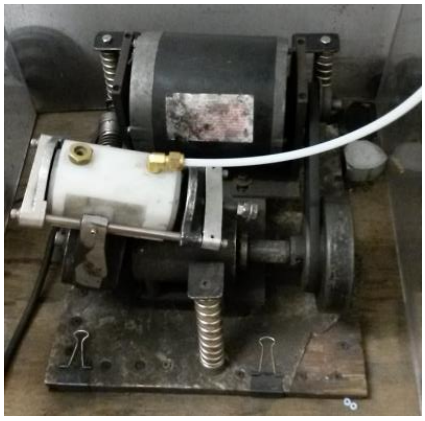

Figure 2.5: Cryomilling setup for $Fe_{50}Se_{25}Te_{25}$ synthesis

The samples produced from milled powders were pressed in a 15 mm diameter tungsten carbide die using a uniaxial pressure of 400 MPa. The pellets were annealed inside the die which was clamped between two stainless steel sheets. The pellets were heated to 700 °C for 1 hour followed by a reduction in temperature to 550°C for 40 hours. The samples were air quenched and allowed to cool inside the die before being extracted. This entire process was performed in an argon purged glove box to prevent oxygen contamination.

Chapter 3

Characterization of FeSe and FeSeTe

3.1 X-ray Diffraction

The phases present in the $Fe_{1.015}Se$ and $Fe_{50}Se_{25}Te_{25}$ pellets were characterized by X-ray diffraction (XRD) using a Rigaku Smart Lab Diffractometer with Cu K-α radiation (λ=0.154 nm). Peak identification and superconducting phase percentage were calculated using PANalytical Highscore Plus diffraction software and the International Centre for Diffraction Data (ICDD) database. The software utilizes the Rietveld Method to calculate phase percentages from the XRD results [21].

3.2 Scanning Electron Microscopy

Scanning electron microscopy was chosen to examine the microstructure of the samples. It was important to determine the amount of porosity in the samples, which could depend on the milling and annealing conditions. A JEOL JSM-6010PLUS/LA scanning electron microscope (SEM) was used to characterize the internal structure of the pellets. Energy-dispersive X-ray spectroscopy (EDS) was used to determine the amount of Fe, Se, and Te present in the samples after annealing.

3.3 Transport

Transport measurements were performed on the samples to determine their superconducting properties. These properties include the superconducting transition temperature and the upper critical field. Sample sizes were around 1 square centimetre. Measurements of the temperature dependence of resistivity over a range from 3 K to 300 K

were performed using the linear four point probe method with a 9 Tesla Quantum Design Physical Property Measurement System (PPMS). This measurement can be used to determine the superconducting transition temperature by looking at the intersection where the material goes from a regular resistivity behaviour to the superconducting behaviour. All temperature dependent measurements were performed while heating through the transition temperature. Contacts to the samples were made with gold coated pogo pins.

3.4 Magnetization

Magnetization measurements were performed to determine the superconducting properties of the sample. Field cooled (FC) and zero field cooled (ZFC) magnetization measurements versus temperature were performed using a Quantum Design MPMS SQUID VSM with a cooling field of 100 Oersted. By looking at the transition of the magnetization where the moment starts to decrease versus temperature we can then determine where the material begins to exhibit superconducting behaviour.

3.5 Critical Current

Critical current measurements were performed using the AC Transport option of the Quantum Design PPMS. The current was ramped until a voltage was observed in the sample, and then, the test was halted. Voltage criterion was calculated using the electric field criterion of E_c=0.1μV/cm with a voltage lead separation of 2 mm which results in an E_c=0.5μV/cm. The critical current value was taken by using the intersection of the voltage criterion and the measured voltage value.

Chapter 4

High Upper Critical Field of β-FeSe Processed by Mechanical Alloying

The β-FeSe phase is highly sensitive to stoichiometry; therefore, multiple iterations of sample composition and milling conditions were tested. A small stoichiometric window for superconductivity is known to exist in the β-FeSe phase which suggests a Se deficient composition [12]. $Fe_{1.015}Se$ was chosen due to it being on the lower end of the stoichiometric window which would still allow for the β-FeSe phase to occur while allowing for the presence of iron impurities. High energy SPEX ball milling was initially tested as the mechanical alloying process but no superconducting samples could be produced due to the presence of high iron impurities. A planetary ball milling process was adopted due to less abrasion of the milling vial wall and media which resulted in a lower amount of iron impurities. The purpose of annealing the pellets inside the tungsten carbide die was to prevent excessive expansion in the pellets due to the relatively low boiling point of selenium (685 °C). Samples annealed without the die lost selenium which altered the composition such that it was outside of the superconducting region.

4.1 Scanning Electron Microscopy

Scanning electron microscopy shows that the $Fe_{1.015}Se$ pellets are dense and relatively free of large pores as shown in Figure 4.1.

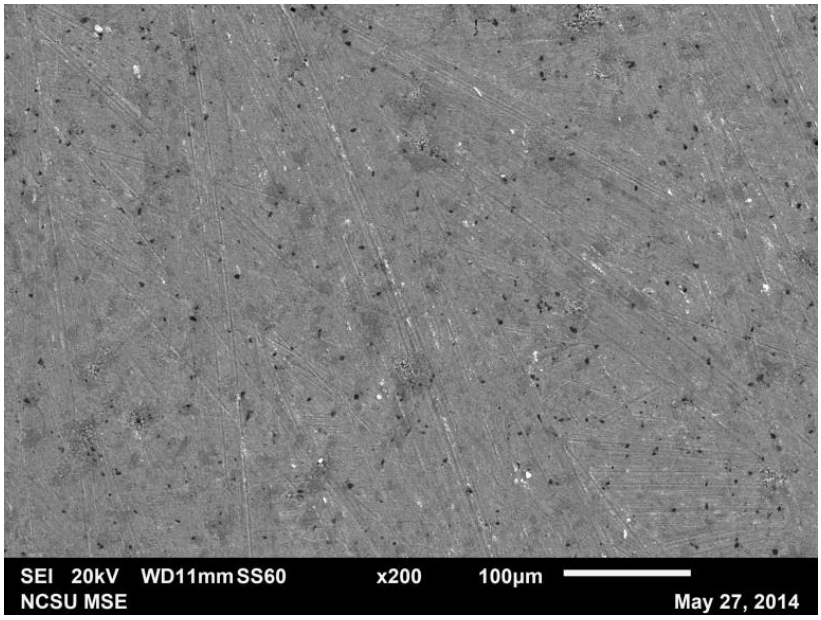

Figure 4.1: Representative SEM image of the internal microstructure of the $Fe_{1.015}Se$ pellets

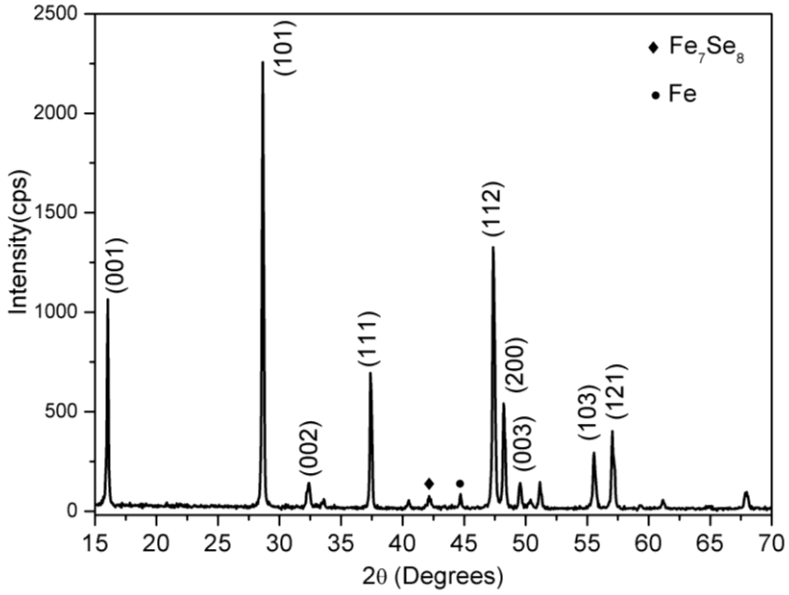

Figure 4.2: XRD spectrum for $Fe_{1.015}Se$ pellets. Impurities are marked above the peaks.

4.2 X-ray Diffraction

XRD results for the $Fe_{1.015}Se$ pellets are shown in Figure 4.2. The pellets consist mostly of the superconducting tetragonal phase, β-FeSe, with a small amount of impurity phases including Fe_7Se_8 and pure Fe. The β-FeSe tetragonal phase volume percentage of the pellets was calculated to be ~94 % using the Rietveld Method [21]. The superconducting phase percentage is much higher than those reported in the literature for other ball milled samples [18, 19]. Fe impurities accounted for ~1.5% of the total sample. Also present in the sample was the non-superconducting hexagonal FeSe phase which accounted for ~4.5% of the sample.

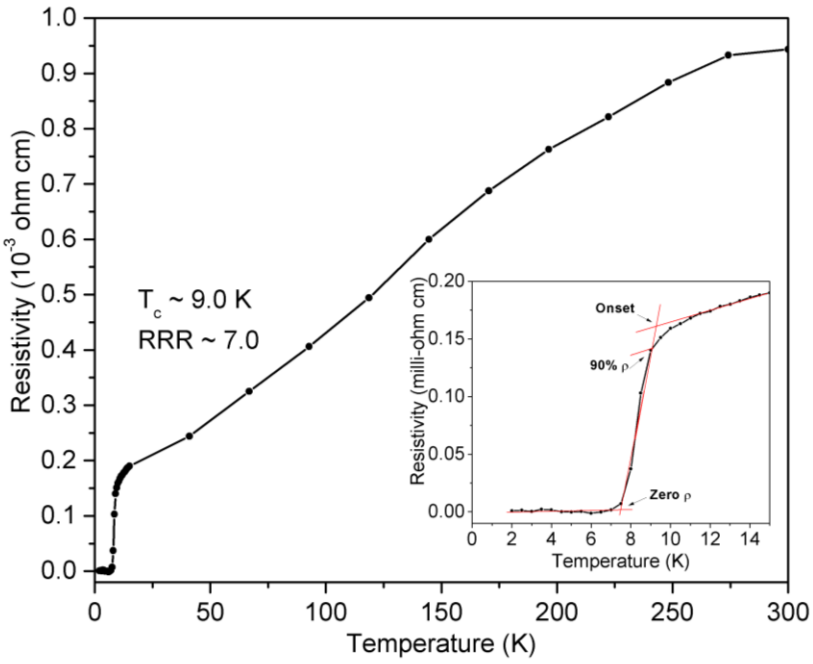

Figure 4.3: Temperature dependence of resistivity for $Fe_{1.015}Se$ pellets. The inset shows an expanded view of the superconducting transition. The overlaid (red) lines show how the transition temperatures at onset, 90% ρ, and zero ρ were determined.

4.3 Transport

Figure 4.3 shows the temperature dependence of resistivity for the $Fe_{1.015}Se$ pellets. The transition temperature (T_c^{onset}) was determined by the intersection of the two extrapolated lines, one from the linear region before the transition and the other from the straightest portion of the transition, as shown in the inset of Figure 4.3. T_c^{onset} for the $Fe_{1.015}Se$ pellets was determined to be 9.0 K, which is similar to those of other ball milled samples [17-19]. Zero resistivity is achieved at 7.8 K which results in a superconducting transition width ΔT of 1.2 K. This ΔT is considerably smaller than those reported in the literature for other ball-milled samples and is believed to arise from the high superconducting phase percentage of the sample [17-19].

The residual resistivity ratio (RRR) was calculated by taking the ratio of the normal state resistivity at 300 K and the resistivity just before the transition temperature in zero field. The $Fe_{1.015}Se$ pellets exhibited a RRR value of 7.0 which suggests toward a high purity sample.

Magnetoresistance measurements were performed up to 9 T on the $Fe_{1.015}Se$ pellets and are presented in Figure 4.4. T_c for each field was taken similar to the inset of Figure 4.3. Figure 4.5 shows a plot of superconducting transition temperatures versus magnetic field used to calculate upper critical field.

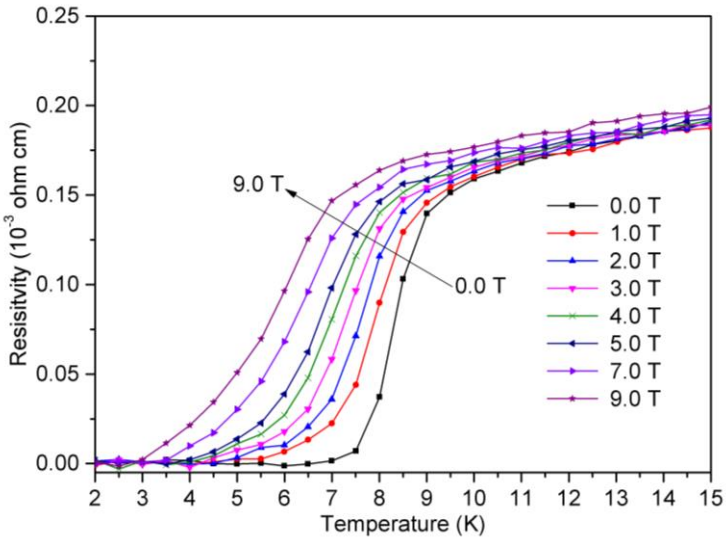

Figure 4.4: Temperature dependence of resistivity for the $Fe_{1.015}Se$ pellets under different applied magnetic fields up to 9 T.

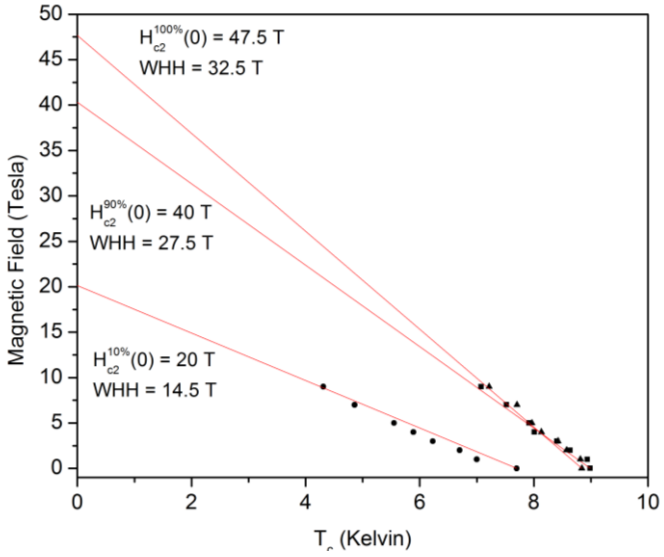

Figure 4.5: Upper critical field linear extrapolation for the $Fe_{1.015}Se$ pellets at 100%, 90%, and 10% ρ. $H_{c2\|c}$ determined by linear extrapolation and the WHH method are shown.

Using linear extrapolation, the $H_{c2\|c}$ (onset) was calculated to be 47.5 T and the $H_{c2\|c}$ (90%) and $H_{c2\|c}$ (0%) were calculated to be 40 T and 20 T, respectively. When compared to literature

values for $H_{c2\|c}$ (90%), these calculated values for $H_{c2\|c}$ (90%) are comparable to those reported for single crystal samples (Table 4.1).

Table 4.1: Comparison of the upper critical field characteristics, $H_{c2\|c}$ calculated from linear extrapolation and the WHH method, of FeSe samples reported here to those presented in the literature along with their reported T_c values and synthesis method. Values with an asterisk (*) were calculated from given plots in the literature. Properties for this study are listed first.

T_c (K)	dH_{c2}/dT_c (T/K)	$H_{c2}(0)$ (90% ρ) [Linear]	$H_{c2}(0)$ (90% ρ) [WHH]	Synthesis Method	Reference
9	**-4.45**	**40T**	**27.5T**	**Ball Milling**	**Current Work**
15.1	-3.33	Exceeds Pauli Limit (1.84 K/T)	N/A	Gas Diffusion	[22]
10	N/A	28 T	19.3 T	PIT	[23]
10.5	-2.72*	32 T	21.7 T*	Diffusion PIT	[24]
~11.5*	-3.65	~27.5 T*	29 T	Single Crystal	[25]
~11.5*	-3.5	N/A	31 T	Single Crystal	[25]
~11*	N/A	N/A	30 T	Single Crystal	[25]
~10.5*	N/A	N/A	28 T	Single Crystal	[25]
9.8	-3	33 T*	18 T	Single Crystal	[26]

The H_{c2} characteristics of the samples were analyzed using the Werthamer–Helfand–Hohenberg (WHH) model which gives $H_{c2}(0) = -0.693 * T_c * \frac{dH_{c2}(T)}{dT}$; $(T = T_c)$ [27]. $H_{c2\|c}$ values for the onset, 90% ρ, and zero ρ were determined to be 32.5, 27.5, and 14.5 T,

respectively. The onset and 90% H_{c2} values for the ball milled sample are on the same order as that for single crystals with similar superconducting phase percentage.

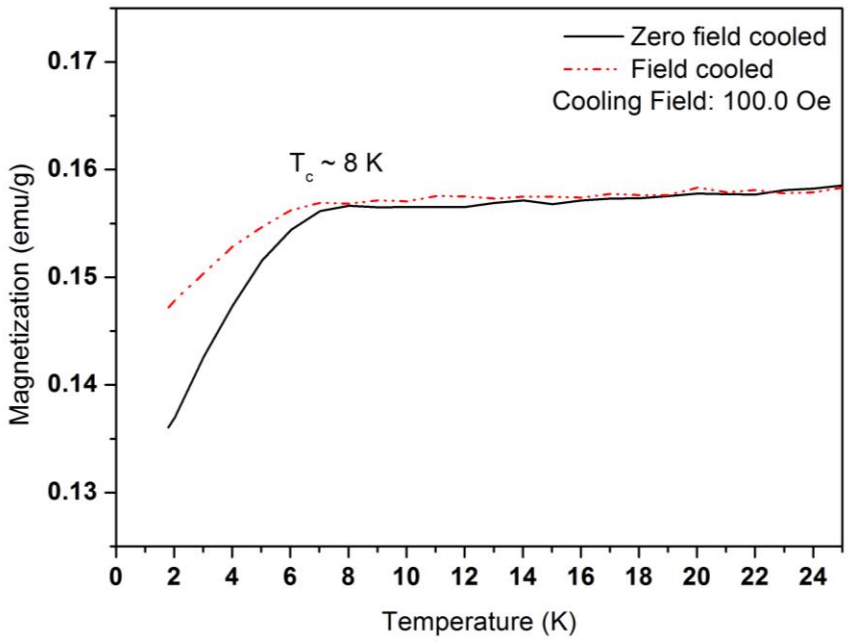

Figure 4.6: Zero field and field cooled magnetization versus temperature measurements for $Fe_{1.015}Se$ pellets.

4.4 Magnetization

Zero field cooled (black solid line) and field cooled (red dashed line) magnetization measurements are shown in Figure 4.6. T_c^{onset} was taken in the zero field cooled case when the plot started to downturn which resulted in a T_c^{onset} of ~8 K. This is lower than that of the T_c^{onset} taken from the resistivity measurements which is due to the sample not consisting entirely of

the superconducting sample. The positive magnetization is attributed to the presence of excess iron in the sample as shown in the XRD results in Figure 4.2.

Chapter 5

Enhancement of the Superconducting Properties of the Ternary FeSeTe via High Energy Ball Milling

5.1 Introduction

More complex iron based superconducting alloys have shown to exhibit higher critical temperatures and upper critical fields. After success with producing the superconducting binary FeSe alloy, the ternary FeSeTe was seen a suitable candidate for the mechanical alloying synthesis. With a lower sensitivity to the stoichiometry, the superconducting phase is much easier to obtain utilizing a mechanical alloying process. Planetary ball milling, high energy SPEX milling, and cryomilling processing techniques were utilized to synthesis the ternary FeSeTe. The superconducting properties of the samples were characterized by magnetization and resistivity as a function of temperature and applied magnetic field.

5.2 Scanning Electron Microscopy

Scanning electron micrographs at 100X, 500X, 1000X, and 2500X were taken of each of the three ball milling conditions to look at the overall microstructure of the sample.

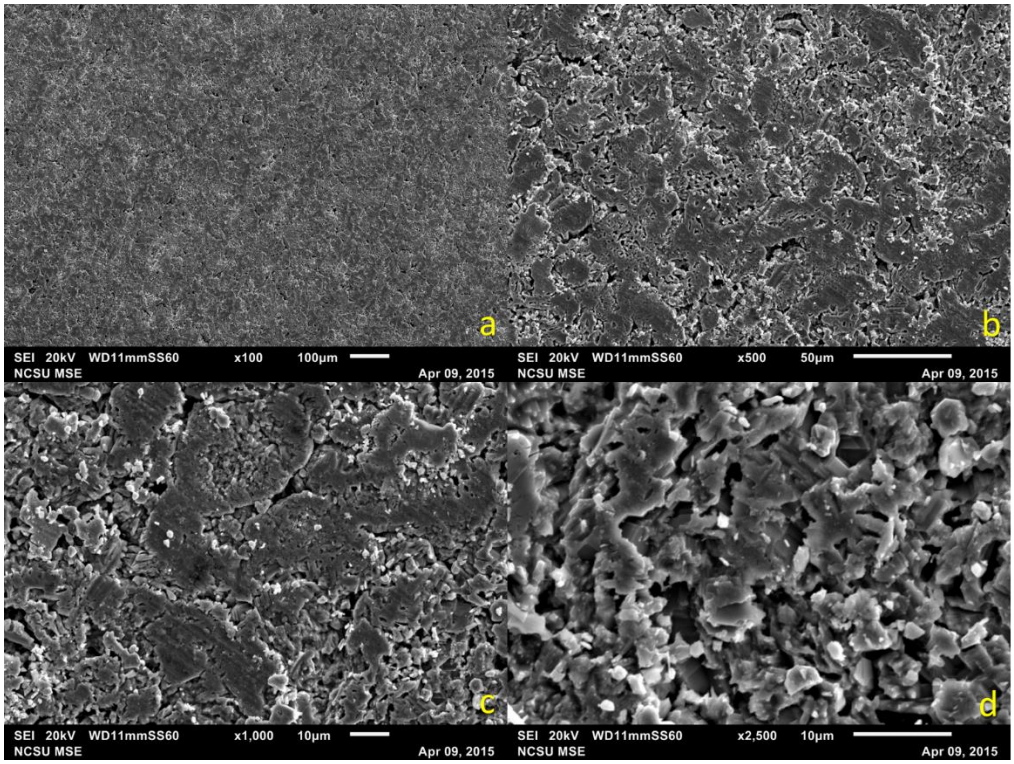

Figure 5.1: Scanning electron micrographs at 100X (a), 500X (b), 1000X (c), and 2500X (d) of the planetary balled milled $Fe_{50}Se_{25}Te_{25}$ sample

As seen in Figure 5.1, the planetary ball milled sample seems free of large pores and fairly dense at 100X (a) and only a small amount of porosity is seen at 500X (b) and 1000X (c). The microstructure at 2500X (d) looks very sharp and appears to be made of layers that are stacked on top of each other which is the typical type of microstructure for β-FeSe. A fair amount of porosity can be seen at 2500X (d) as compared to the lower magnifications. EDS analysis shows that the planetary ball milled sample is 46.92wt% Fe, 24.41wt% Se, and 28.66wt% Te which is slightly off of the original intended $Fe_{50}Se_{25}Te_{25}$ stoichiometry.

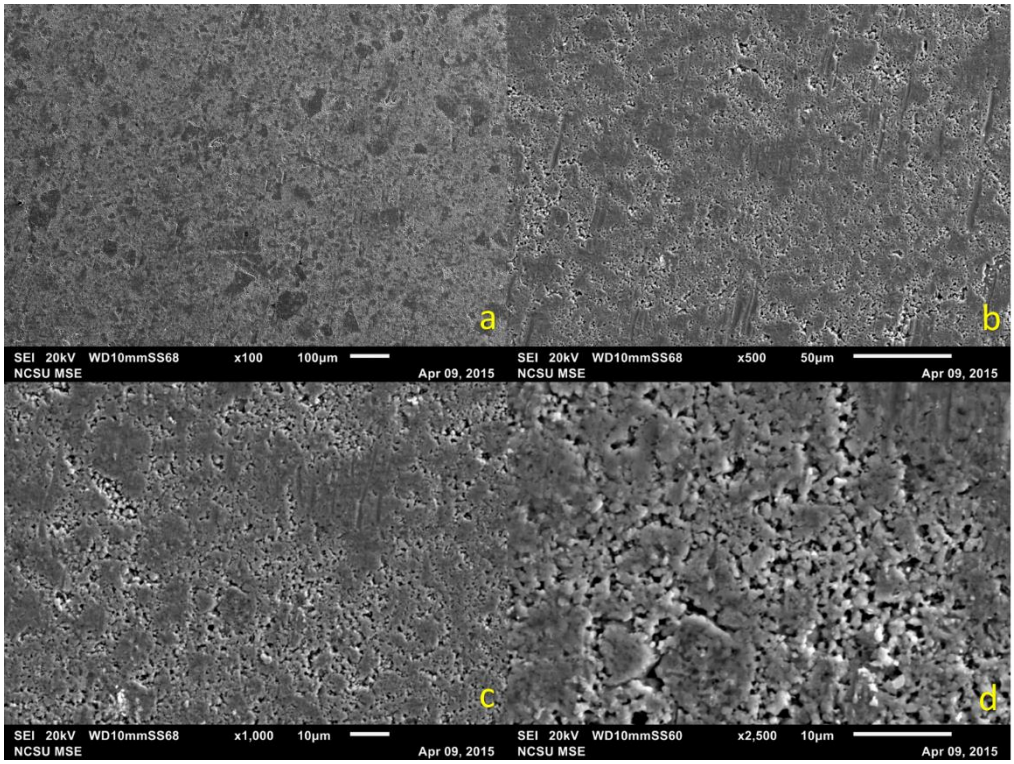

Figure 5.2: Scanning electron micrographs at 100X (a), 500X (b), 1000X (c), and 2500X (d) of the high energy SPEX milled $Fe_{50}Se_{25}Te_{25}$ sample

In Figure 5.2, the SPEX milled sample is also free of any large pores and looks to be denser than the planetary ball milled sample at 500X (b). At 2500X, the sample has far less porosity compared to the planetary ball milled sample as the particles are fused together and look very smooth. This could be due to smaller particle size as a result of the higher energy ball milling process. The smaller particles would result in a larger surface area for sintering. EDS shows that the SPEX milled sample is 48.14wt% Fe, 23.16wt% Se, and 28.7wt% Te which is even more off of the original $Fe_{50}Se_{25}Te_{25}$ stoichiometry than the planetary ball milled sample. This could be attributed to either a loss of selenium during milling and annealing.

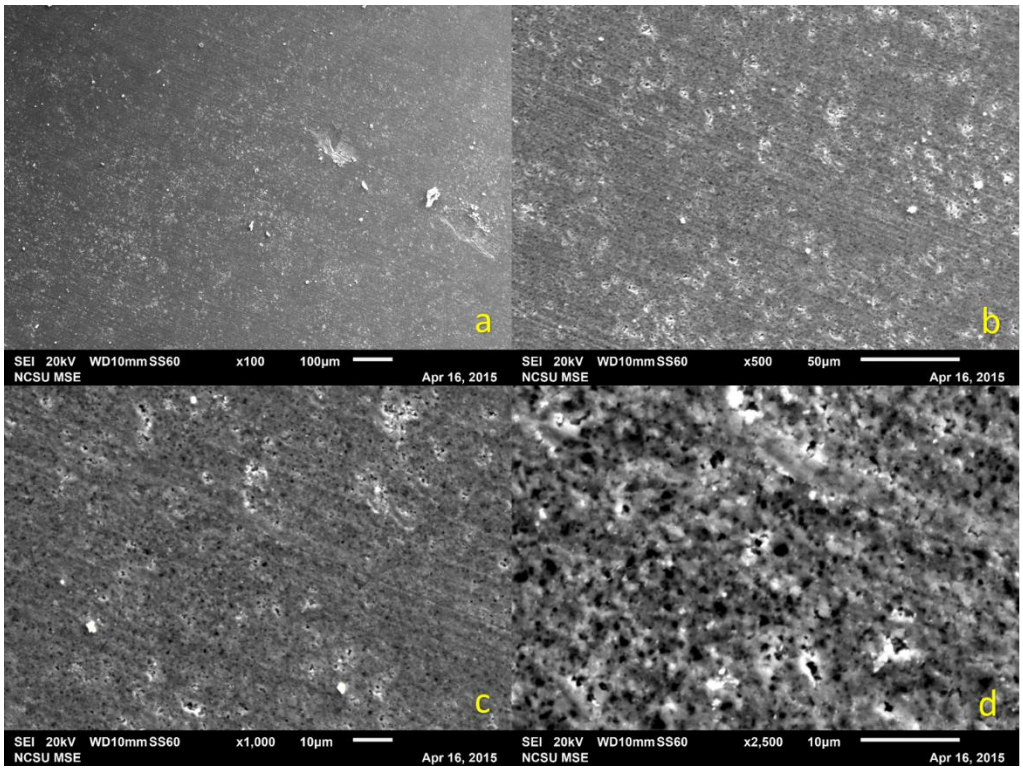

Figure 5.3: Scanning electron micrographs at 100X (a), 500X (b), 1000X (c), and 2500X (d) of the cryomilled $Fe_{50}Se_{25}Te_{25}$ sample

In Figure 5.3, the cryomilled sample is dense and free of large pores at 500X (b) but smaller pores can be resolved at 2500X (d). The porosity seems to be similar in size and evenly distributed through the sample. This porosity is most likely due to the cryomilling process which is due to the argon that is introduced into the lattice of the powder during milling. Since the milling process is performed at cryogenic temperatures, the argon (atmosphere present in the vial while milling) is solid. The milling process introduces the solid argon into the lattice via deformation from the milling media. When the samples are annealed, the argon expands which results in the porosity observed in the samples.

5.3 Transport

Figure 5.4 shows the temperature dependence of resistivity for the planetary ball milled sample. The inset shows an expanded view of the superconducting transition where two intersecting black lines are used to estimate the superconducting onset temperature (T_c^{onset}). One line is drawn through the linear part of the curve before the transition and the other is drawn through the linear portion of the transition to zero resistivity. T_c^{onset} at zero field for the planetary ball milled sample was estimated to be ~13.7K. Zero resistivity is estimated to be around ~12.4K which results in a sharp transition with a ΔT of ~1.3K.

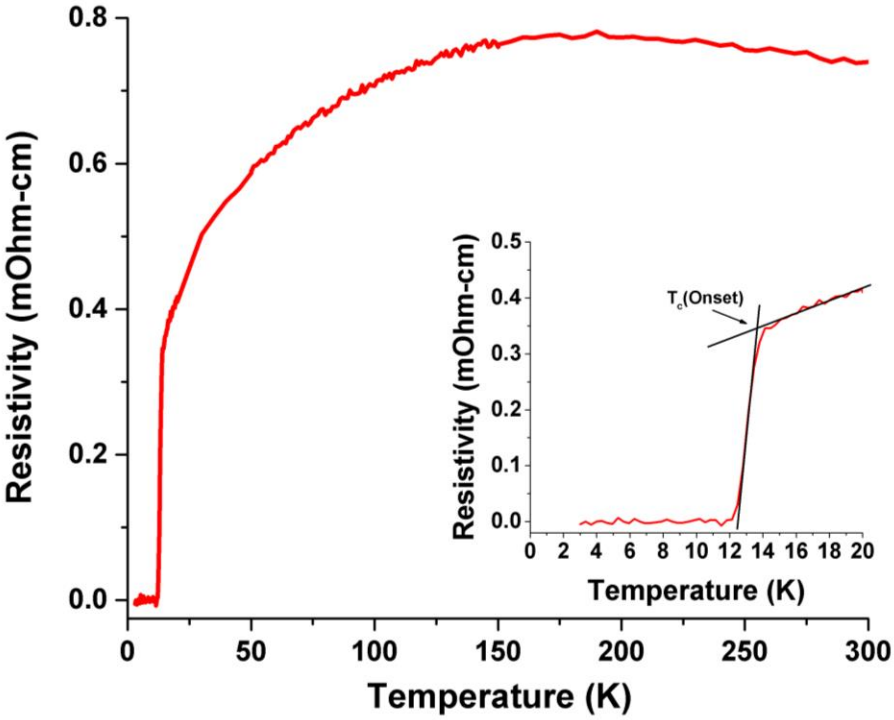

Figure 5.4: Temperature dependence of resistivity from 3K to 300K for planetary ball milled $Fe_{50}Se_{25}Te_{25}$. The inset shows an expanded view from 3K to 20K with the overlaid black lines showing how the transition temperature at onset was taken.

The temperature dependence of resistivity for the high energy SPEX milled sample is shown in Figure 5.5. The inset shows that the T_c^{onset} at zero field is approximately ~14.3K which is higher than that of the planetary ball milled sample. The zero resistivity temperature is estimated to be around ~11.9K which results in a transition gap of around $\Delta T \sim 2.4K$ which is larger than the planetary ball milled sample. The resistivity from 300K to around ~175K slightly increases for both the planetary ball milled and high energy SPEX milled samples. After this transition, the samples start to exhibit metallic behavior down to the superconducting transition. The resistivity before the superconducting transition and at room temperature of the SPEX milled sample is almost twice that of the planetary ball milled sample. This could be due to a higher defect concentration in the SPEX milled sample introduced during the energy ball milled process.

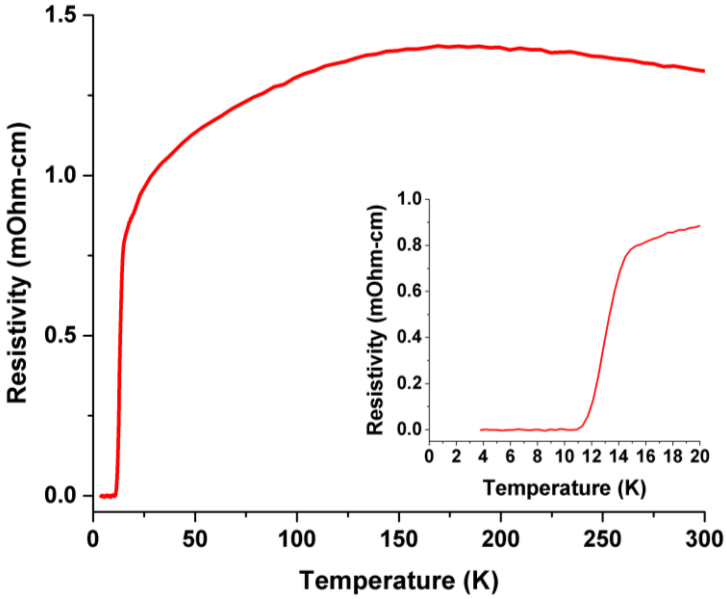

Figure 5.5: Temperature dependence of resistivity from 4K to 300K for high energy SPEX milled $Fe_{50}Se_{25}Te_{25}$. The inset shows an expanded view from 4K to 20K.

Temperature dependence of resistivity for the cryomilled sample is shown in Figure 5.6. The T_c^{onset} at zero field was estimated to ~14.1K which is very similar to the high energy SPEX milled powder at room temperature. No significant difference is seen in the T_c^{onset} with a difference in the milling temperature but in general the high energy ball milling process increases the T_c^{onset} by ~0.5K. This could be attributed to the high energy ball milling process resulting in a higher concentration of the superconducting phase. The zero resistivity at zero field was estimated to be ~12.1K which results in a ΔT of ~2K. This small ΔT is seen in all three milling techniques. The resistivity from 300K to around ~225K exhibits semiconducting behavior then start to exhibit metallic behavior down to the superconducting transition. The magnitude of the resistivities for the cryomilled samples is over 4 times larger than that of the

planetary ball milled sample and over 2 times larger than the high energy SPEX milled sample. This larger resistivity for the high energy ball milled samples is due to a larger scattering effect due to a higher concentration of defects introduced during the milling process.

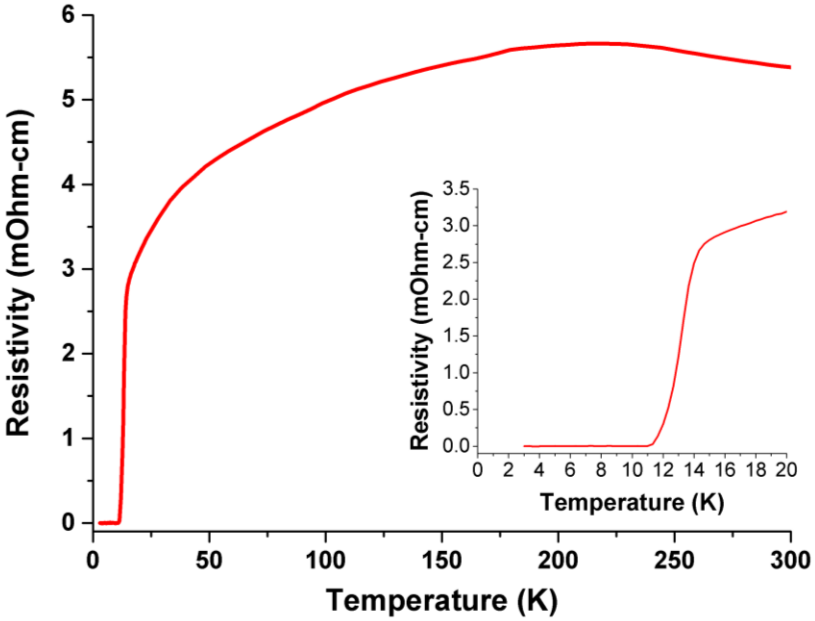

Figure 5.6: Temperature dependence of resistivity from 3K to 300K for cryomilled $Fe_{50}Se_{25}Te_{25}$. The inset shows an expanded view from 3K to 20K.

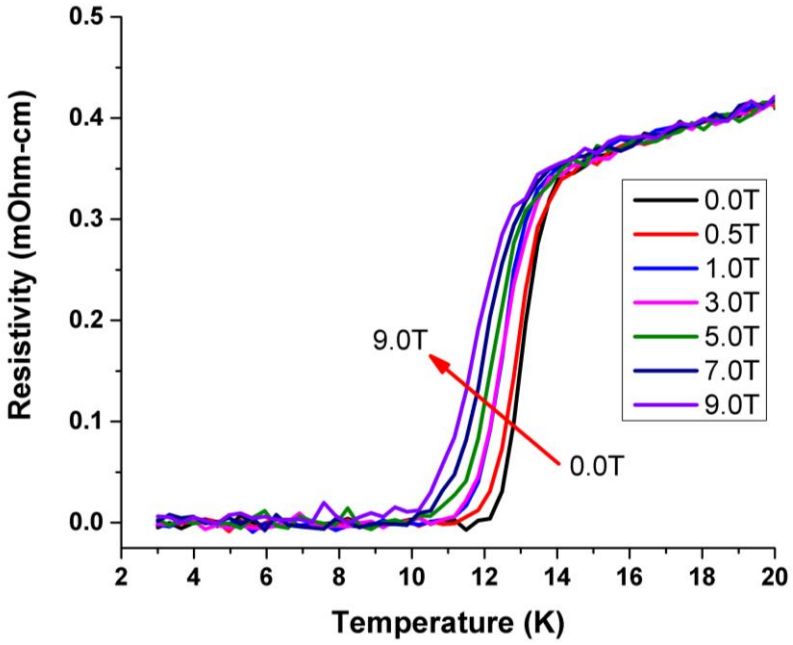

Figure 5.7: Temperature dependence of resistivity for planetary ball milled $Fe_{50}Se_{25}Te_{25}$ under different applied magnet fields up to 9 T

Magnetotransport measurements were run for each of the three milling conditions. Figure 5.7 shows the temperature dependence of resistivity from 0 to 9 Tesla. At 9 T, the sample has a T_c^{onset} of ~12.7K and is still able to reach zero resistivity at ~10.7K. By plotting the T_c^{onset} at each of the applied fields versus the applied magnet field, the upper critical field, $H_{c2\|c}(0)$, can be linearly extrapolated to zero kelvin which can give insight into the maximum field for which the sample can maintain superconductivity. For the planetary ball milled sample, the $H_{c2\|c}(0)$ was approximated to be ~134 Tesla with the linear approximation having a strong correlation to the data. Utilizing the Werthamer–Helfand–Hohenberg (WHH) model which says that $H_{c2}(0) = -0.693 * T_c * \frac{dH_{c2}(T)}{dT}$; $(T = T_c)$ [27], we are able to calculate an alternative upper critical field using the slope of the linear approximation and the superconducting onset

transition temperature. Assuming that the T_c^{onset} is ~13.7K and the slope of the linear approximation is -9.82 K/T, the WHH method yields an $H_{c2||c}(0)$ ~ 93.5 T. This $H_{c2||c}(0)$ value is lower than that of the linear approximation but tends to be more accurate.

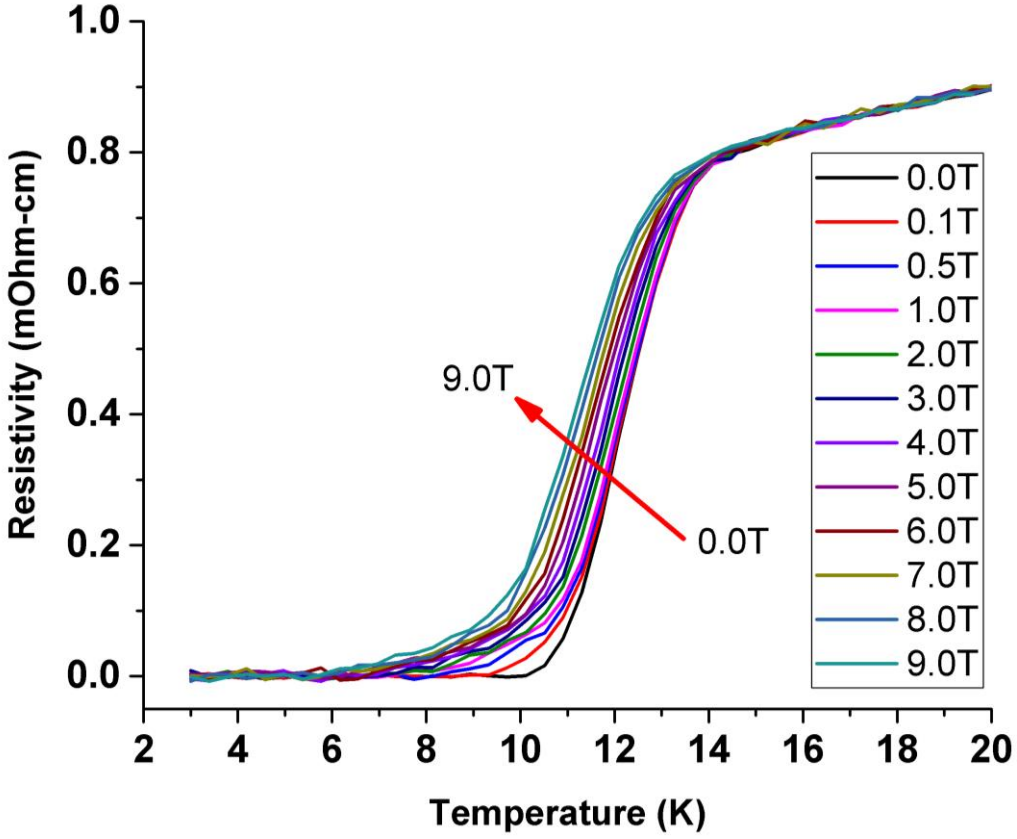

Figure 5.8: Temperature dependence of resistivity for high energy SPEX milled $Fe_{50}Se_{25}Te_{25}$ under different applied magnet fields up to 9 T

Figure 5.8 shows the temperature dependence of resistivity from 0 to 9 Tesla for the high energy SPEX milled sample. At 9 T, the T_c^{onset} is still approximately ~12.7 K which is what was estimated for the planetary ball milled sample. The largest difference between the samples is the zero resistivity temperature at 9 T which is around ~5.5 K for the SPEX milled sample

which is almost a 7K difference. For the SPEX milled sample, the $H_{c2||c}(0)$ was estimated to be ~159.7 T using the linear extrapolation model. Using a slope of -11.721 K/T and a T_c^{onset} of 14.3 K, the WHH estimation of the $H_{c2||c}(0)$ is 116.2 T which is a 20 T increase over the planetary ball milled sample. This may be due to the increase in defects present in the sample from the high energy SPEX milling.

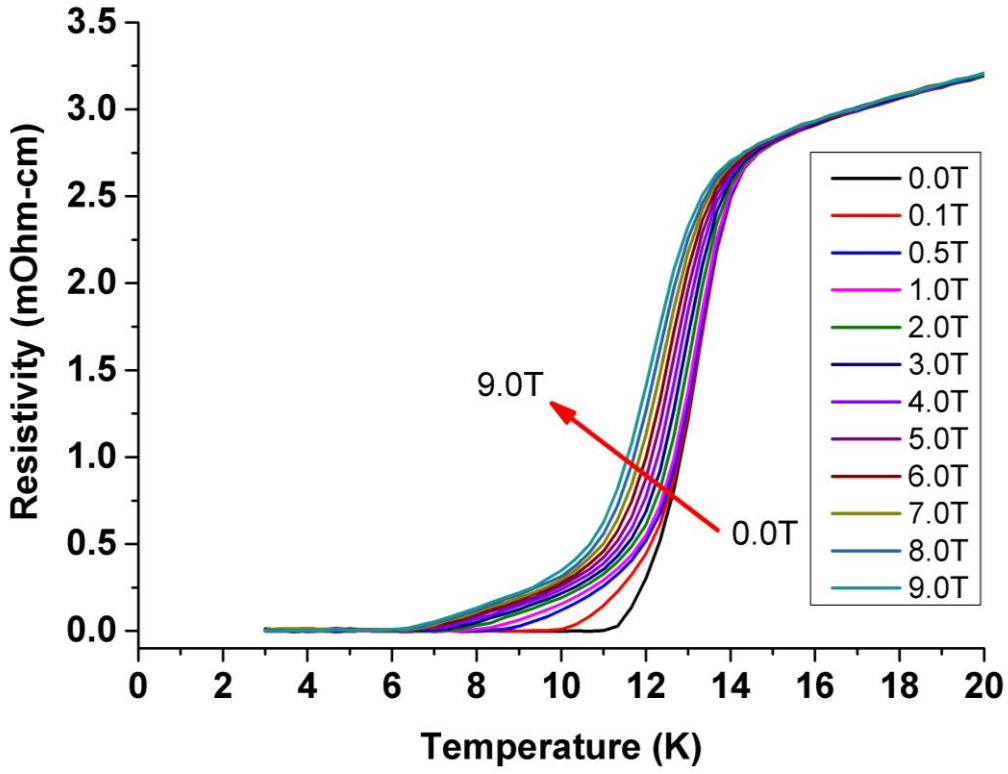

Figure 5.9: Temperature dependence of resistivity for cryomilled $Fe_{50}Se_{25}Te_{25}$ under different applied magnet fields up to 9 T

The T_c^{onset} for the cryomilled sample at 9 T was estimated to be ~13.6K as seen from Figure 5.9. This slightly higher than the two previous samples. The zero resistivity was estimated to

be ~6.6K which results in a difference of around ~6.8K which is the largest ΔT seen at 9 T in all three milling processes. The $H_{c2||c}(0)$ for the cryomilled sample was estimated using linear extrapolation to be around ~167T which is significantly higher than that of the planetary ball milled and on par with the high energy SPEX milled at room temperature. By using a slope of -11.847 K/T and a T_c^{onset} of 14.1K, the WHH estimation for the $H_{c2||c}(0)$ was around ~115.8T which is very similar to the high energy SPEX milled sample. Changing to a cryogenic temperature for the high energy ball milling process seems to have no effect in the $H_{c2||c}(0)$.

5.4 Magnetization

The temperature dependence of magnetization in field cooled and zero field cooled for the planetary ball milled sample in the transition region is shown in Figure 5.10. The T_c^{onset} for magnetization is taken when the zero field cooled line starts to curve downward towards a negative moment.

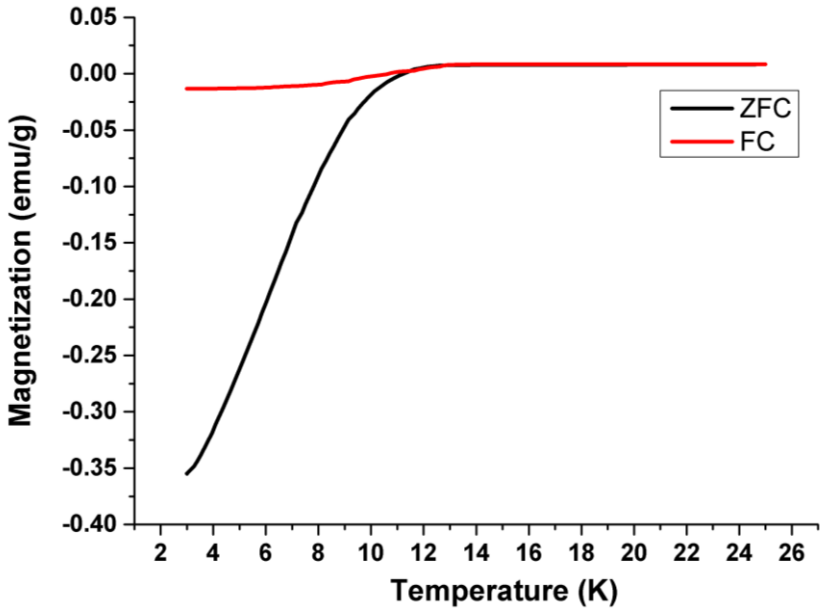

Figure 5.10: Field cooled (red) and zero field cooled (black) temperature dependence of magnetization from 3K to 25 K of planetary ball milled $Fe_{50}Se_{25}Te_{25}$

For the planetary ball milled sample, the T_c^{onset} is estimated to be ~12.6K which is less than the T_c^{onset} approximated by the temperature dependence of resistivity. This is due to the fact that the magnetization measurement is a global characterization of the sample whereas the resistivity measurement only requires superconducting pathways to run through the sample therefore the entire sample may not be entirely superconducting. In this case, a small volume fraction of the sample which is non-superconducting would result in a lower T_c^{onset} in magnetization measurements than in the resistivity ones.

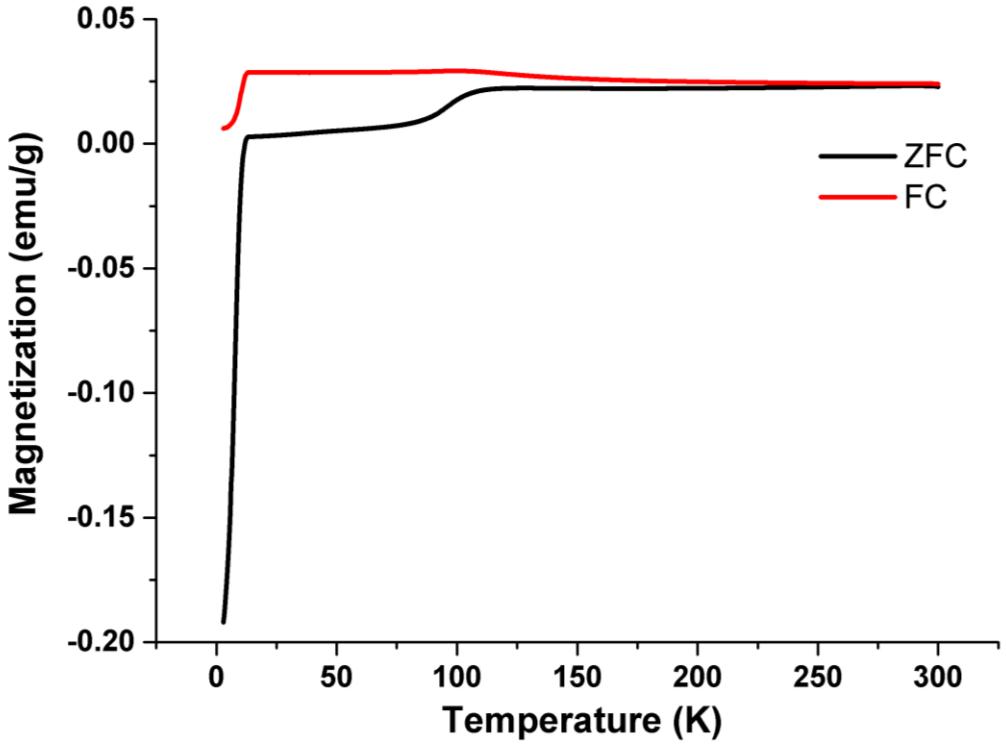

Figure 5.11: Field cooled (red) and zero field cooled (black) temperature dependence of magnetization from 3K to 300 K of planetary ball milled $Fe_{50}Se_{25}Te_{25}$

As seen in Figure 5.11, there is an anomaly in the field cooled and zero field cooled magnetization around ~120K where it seems to transition and then return to a linear slope. A tetragonal-triclinic phase transformation is known to occur around ~105K [10] and a tetragonal-orthorhombic phase transformation around ~70K [28]. This strange magnetic anomaly has been seen in other FeSeTe samples from other processing techniques but does not correlate to a structural or magnetic transition [29].

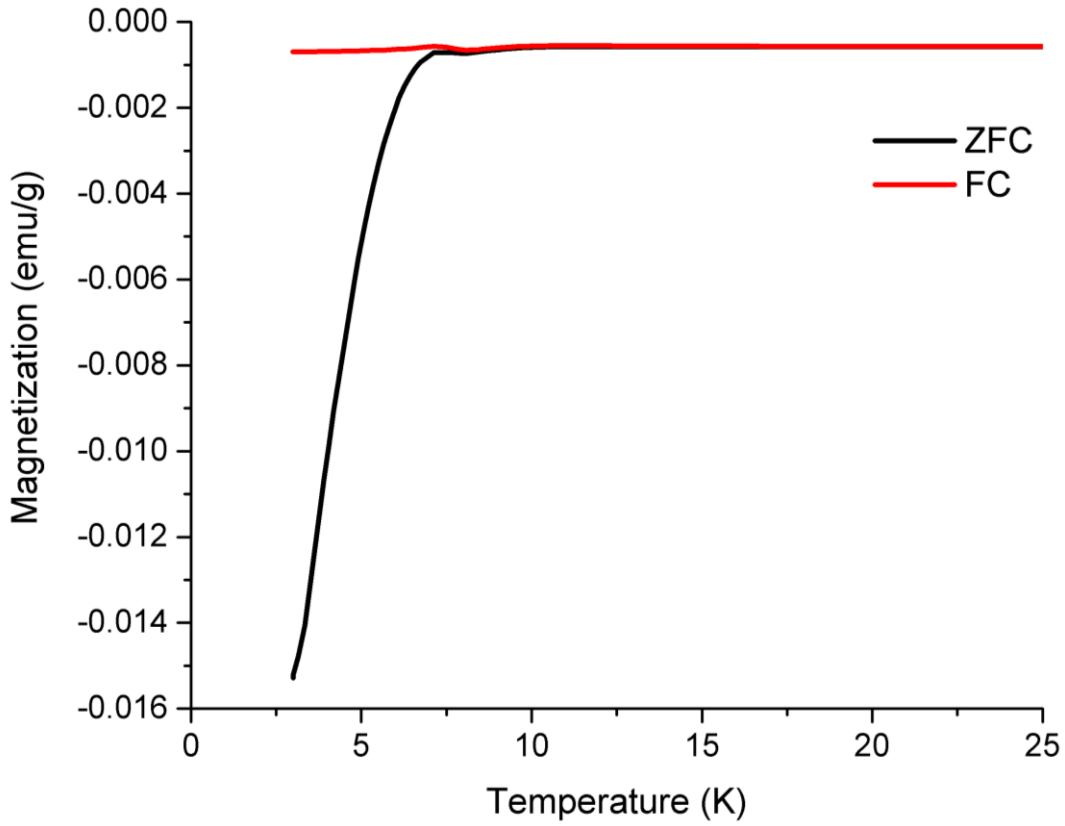

Figure 5.12: Field cooled (red) and zero field cooled (black) temperature dependence of magnetization from 3K to 25 K of high energy SPEX milled $Fe_{50}Se_{25}Te_{25}$

The temperature dependence of magnetization for the high energy SPEX milled sample is shown in Figure 5.12. The magnetization seems to have two transitions at lower temperatures. The first transition is around ~10.3K which is where we would expect the superconducting transition to occur. This transition seems to end around ~8K where the magnetization then increases slightly until ~7.1K. This second transition of ~7.1K seems to demonstrate the traditional superconducting transition behavior as the moment continues to sharply decrease due to diamagnetism. There has been no report of this is the literature and further

characterization such as low temperature high resolution X-ray diffraction should be performed to determine what type of transition is occurring.

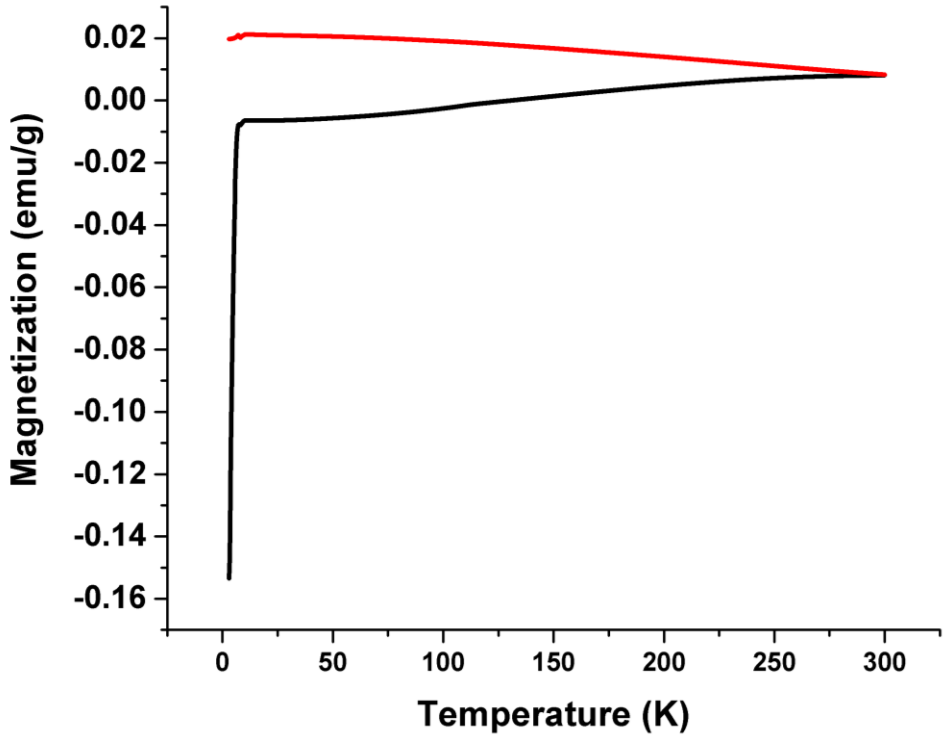

Figure 5.13 Field cooled (red) and zero field cooled (black) temperature dependence of magnetization from 3K to 300 K of high energy SPEX milled $Fe_{50}Se_{25}Te_{25}$

Figure 5.13 shows the temperature dependence of magnetization up to 300K for the high energy SPEX milled sample. The same superconducting transition is seen except that the zero field cooled and field cooled lines do not lie on top of each other down to the superconducting transition and start to diverge around ~275K. No other transitions are seen in the high energy SPEX milled sample unlike the planetary ball milled sample which exhibited a transition

around ~120K. The positive magnetization in the field cooled data could be a result of excess ferromagnetic iron from the milling or annealing process.

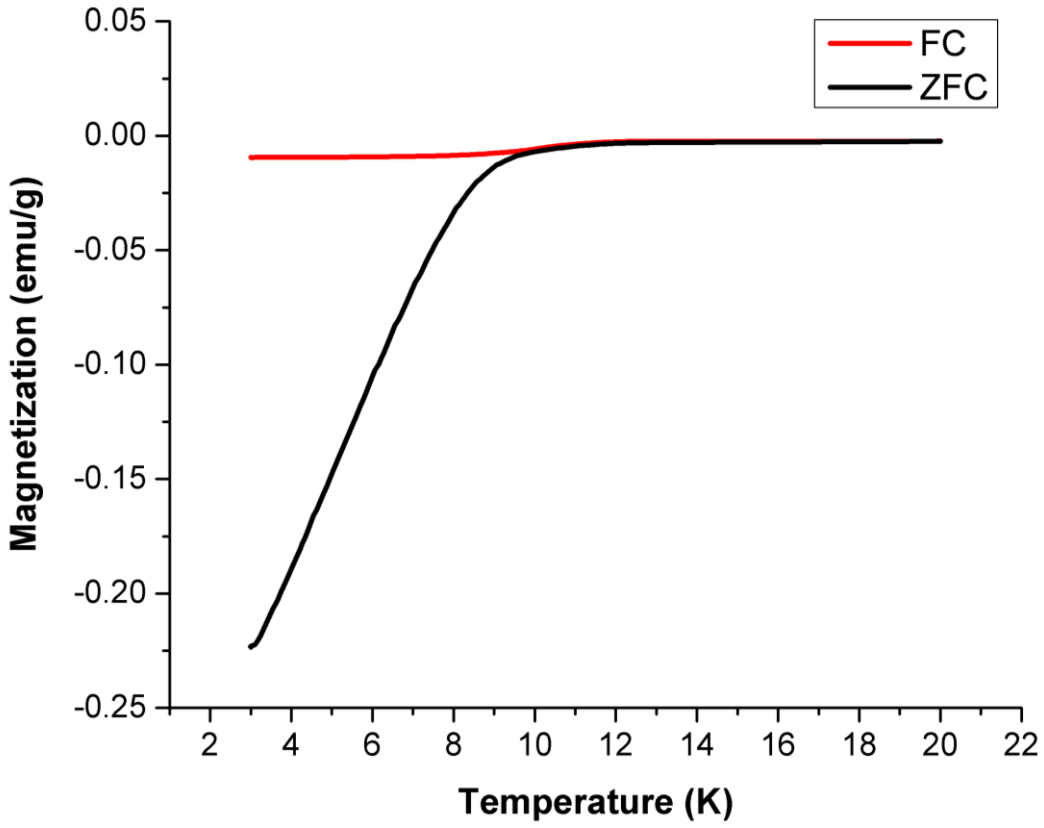

Figure 5.14: Field cooled (red) and zero field cooled (black) temperature dependence of magnetization from 3K to 20 K of cryomilled $Fe_{50}Se_{25}Te_{25}$

The temperature dependence of magnetization for the cryomilled sample is shown in Figure 5.14 with an estimated T_c^{onset} of ~12.9K which is about 2K higher than the high energy SPEX milled sample at room temperature. When compared to the planetary ball milled sample, the T_c^{onset} is within ~0.3K which is interesting due to the fact that one would expect the high energy

SPEX milled and cryomilled samples to be more similar as seen in the temperature dependence of resistivity.

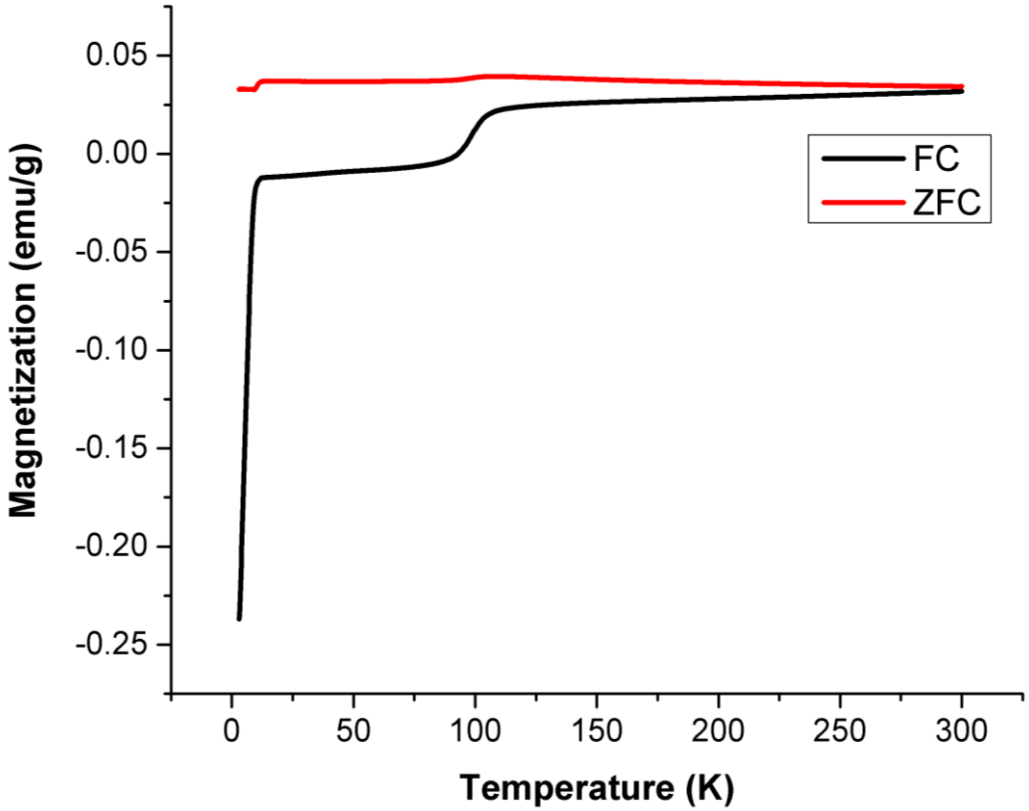

Figure 5.15: Field cooled (red) and zero field cooled (black) temperature dependence of magnetization from 3K to 300 K of cryomilled $Fe_{50}Se_{25}Te_{25}$

As seen in Figure 5.15, the transitions around ~120K and ~70K reappear in the cryomilled sample similar to those in the planetary ball milled sample. These transitions disappeared in the high energy SPEX milled sample and may be due to the extended milling time experienced by the sample. The positive magnetization in the field cooled data is more than likely a result

of excess ferromagnetic iron from the milling or annealing process similar to that of the high energy SPEX milled samples.

5.5 Critical Current

Figure 5.16 shows the critical current measurements for all three milling conditions measured at 5 K. The planetary ball milled sample supported the highest critical current of the three milling process with I_c~935 mA. The high energy SPEX milled sample was able to support ~860 mA whereas the cryomilled sample was only able to support around ~560 mA. This low critical current value could be caused by the porosity seen in the sample which could result in lower connectivity of the superconducting phase.

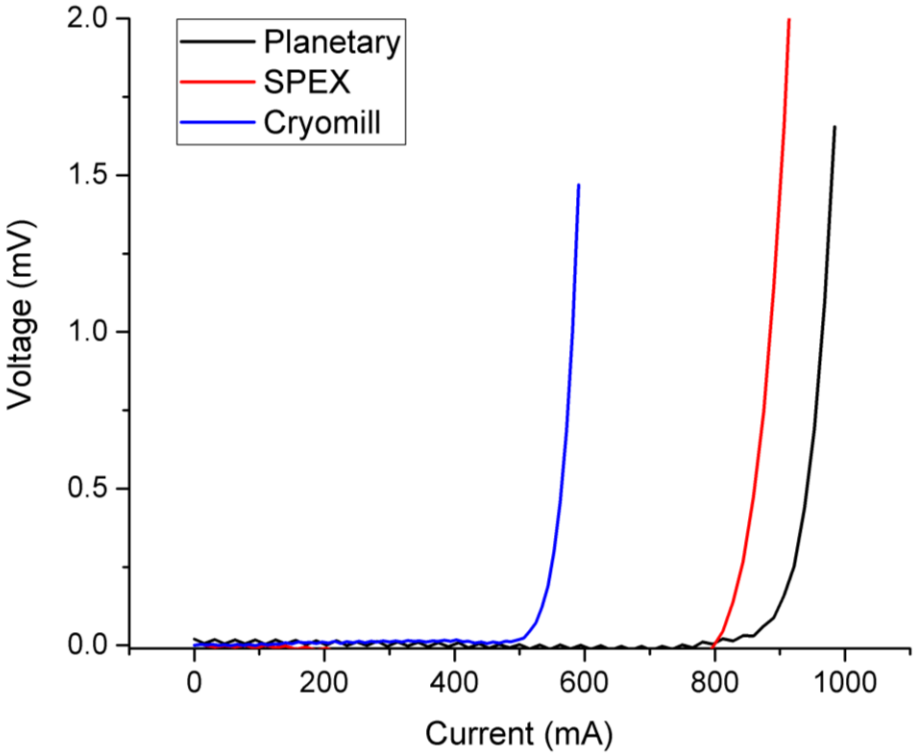

Figure 5.16: Critical current measurements for planetary, SPEX, and cryomilled samples at 5K

5.6 Summary

Table 5.1 shows a summary of the superconducting properties of the $Fe_{50}Se_{25}Te_{25}$ synthesized by planetary ball milling, high energy SPEX milling, and cryomilling. When looking at the supercondcuting transition temperatures, the high energy SPEX milling has the highest critical tempertaure with cryomilling falling close behind. This is most likely due to a higher superconducting phase percentage in the sample due to the higher energy ball milling process. The upper critical fields for the planetary ball milling and cryomilling exceeded 160 T while the planetary ball milling only reached 134 T. This increased upper critical field in the high energy ball milling process is most likely due to the higher defect

concentrations caused by the milling processleading to higher scattering in the material. These properties show that the higher energy ball milling processes result in a better sample. This is contradicted by the critical current data which shows that the planetary ball milling process resulted in the highest critical current followed by the high energy SPEX milling process. The cryomilling process showed a drastic difference in critical current which is mostly due to lower connectivity of the superconducting phase. This possibly could be due to the extra porosity from the argon embeded in the lattice during milling.

Table 5.2: Summary of the superconducting properties of the planetary ball milling, high energy SPEX milling, and cryomilling of $Fe_{50}Se_{25}Te_{25}$

	T_c^{onset} (K)	ΔT (K)	H_{c2} (T)	H_{c2} (WHH) (T)	Critical Current (mA)
Planetary Milling	13.7	1.3	134	93.5	935
High Energy SPEX Milling	14.3	2.4	159.7	116.2	860
Cryomilling	14.1	2	167	115.8	560

Chapter 6

Summary and Future Work

6.1 Summary

The mechanical alloying process was successfully used for the synthesis of both, binary FeSe and the ternary FeSeTe. After overcoming issues with contamination of iron from the milling vial/media, FeSe was synthesized utilizing a planetary ball milling process which resulted in a very pure superconducting sample with enhanced properties. The superconducting transition temperature was found to be ~9K with a ΔT of ~1.2K which is smaller than those reported in the literature. Magnetization measurements supported the superconducting behavior seen along with the transition temperature. The upper critical field for the polycrystalline samples were found to be 40T using the linear extrapolation method and ~27.5T using the WHH method which is on the order of those observed in single crystal samples.

In the case of the FeSeTe, a combination of three separate ball milling processes (planetary, high energy SPEX, and cryomilling) was utilized to synthesize superconducting samples. It was shown that all three milling processes were capable of forming the superconducting phases whether they were fabricated with high or low energy ball milling processes. The cryomilling process resulted in a more porous structure than the other milling processes. The planetary ball milling process resulted in a transition temperature of around ~12.4K with the high energy SPEX process having a slightly higher transition of ~14.3K. The cryomilling process resulted in a transition temperature of ~12.1K which was lower than both

the other process. The upper critical fields of the three milling processes showed the highest values for the cryomilled samples whereas the planetary ball milled samples had the lowest. The temperature difference between the high energy SPEX milling and cryomilling seemed to have little effect on the upper critical filed values. The larger values for the high energy ball milling process is mostly due to higher concentrations of defects in the samples as the upper critical field is a processing dependent property. Magnetization measurements for each milling process supported the transition temperatures as determine by resistivity measurements. Tetragonal-triclinic and tetragonal-orthorhombic phase transitions were seen in the planetary and cryomilling processes but were absent in the high energy SPEX milling process. Critical current measurements show that the planetary ball milled sample supported the highest critical current at 5K follow by the high energy SPEX milled sample. The cryomilled samples showed a much lower critical current value, which can be attributed to the more porous structure of the sample.

6.2 Conclusions

The data presented above demonstrates that mechanically alloying processes are a viable synthesis route for bulk processing of these simple iron based superconducting compounds. The milling processes seem to enhance some of the superconducting properties such as the transition temperature and upper critical field. The high energy processes seem to have a larger enhancement on the properties.

6.3 Future Work

Further work should focus on utilizing the mechanical alloying processes to produce iron based superconductors of more complex chemistries. These higher complexity

compounds often bring with them a higher transition temperature and upper critical field which makes these compounds more useful for potential applications. By utilizing these mechanical alloying processes then powder can be synthesized in bulk for use in wires via a powder in tube method. Special emphasis should be placed on the sintering process to ensure good grain connectivity for higher critical current values.

6.4 References

[1] H. Onnes. The liquefaction of helium. *PROCEEDINGS OF THE KONINKLIJKE AKADEMIE VAN WETENSCHAPPEN TE AMSTERDAM} 11}(1}),* pp. 168-185}. 1908}.

[2] H. K. Onnes. On the sudden rate at which the resistance of mercury disappears. *Akad.Van Wetenschappen 14(113),* pp. 818. 1911.

[3] A. K. Saxena. *High-Temperature Superconductors* 2012.

[4] J. BEDNORZ and K. MULLER. POSSIBLE HIGH-TC SUPERCONDUCTIVITY IN THE BA-LA-CU-O SYSTEM. *ZEITSCHRIFT FUR PHYSIK B-CONDENSED MATTER} 64}(2}),* pp. 189-193}. 1986}. . DOI: {10.1007/BF01303701.

[5] M. WU, J. ASHBURN, C. TORNG, P. HOR, R. MENG, L. GAO, Z. HUANG, Y. WANG and C. CHU. SUPERCONDUCTIVITY AT 93-K IN A NEW MIXED-PHASE Y-BA-CU-O COMPOUND SYSTEM AT AMBIENT PRESSURE. *PHYSICAL REVIEW LETTERS} 58}(9}),* pp. 908-910}. 1987}. . DOI: {10.1103/PhysRevLett.58.908.

[6] Y. Kamihara, T. Watanabe, M. Hirano and H. Hosono. Iron-based layered superconductor la[O1-xFx]FeAs (x=0.05-0.12) with T-c=26 K. *Journal of the American Chemical Society 130(11),* pp. 3296. 2008. . DOI: 10.1021/ja800073m.

[7] A. S. Sefat and D. J. Singh. Chemistry and electronic structure of iron-based superconductors. *MRS Bulletin 36(8),* pp. 614-619. 2011. . DOI: 10.1557/mrs.2011.175.

[8] R. Zhi-An, L. Wei, Y. Jie, Y. Wei, S. Xiao-Li, Zheng-Cai, C. Guang-Can, D. Xiao-Li, S. Li-Ling, Z. Fang and Z. Zhong-Xian. Superconductivity at 55 K in iron-based F-doped layered quaternary compound sm[O 1- x F x] FeAs. *Chinese Physics Letters 25(6),* pp. 2215. 2008. . DOI: 10.1088/0256-307X/25/6/080.

[9] F. Hunte, J. Jaroszynski, A. Gurevich, D. C. Larbalestier, R. Jin, A. S. Sefat, M. A. McGuire, B. C. Sales, D. K. Christen and D. Mandrus. Two-band superconductivity in LaFeAsO(0.89)F(0.11) at very high magnetic fields. *Nature 453(7197),* pp. 903-905. 2008. . DOI: 10.1038/nature07058.

[10] F. Hsu, J. Luo, K. Yeh, T. Chen, T. Huang, P. M. Wu, Y. Lee, Y. Huang, Y. Chu, D. Yan and M. Wu. Superconductivity in the PbO-type structure alpha-FeSe. *Proceedings of the National Academy of Sciences of the United States of America 105(38),* pp. 14262-14264. 2008. . DOI: 10.1073/pnas.0807325105.

[11] S. Medvedev, T. M. McQueen, I. A. Troyan, T. Palasyuk, M. I. Eremets, R. J. Cava, S. Naghavi, F. Casper, V. Ksenofontov, G. Wortmann and C. Felser. Electronic and magnetic

phase diagram of beta-Fe1.01Se with superconductivity at 36.7 K under pressure. *NATURE MATERIALS} 8}(8)},* pp. 630-633}. 2009}. . DOI: {10.1038/NMAT2491.

[12] T. M. McQueen, Q. Huang, V. Ksenofontov, C. Felser, Q. Xu, H. Zandbergen, Y. S. Hor, J. Allred, A. J. Williams, D. Qu, J. Checkelsky, N. P. Ong and R. J. Cava. Extreme sensitivity of superconductivity to stoichiometry in Fe1+delta se. *Physical Review B 79(1),* pp. 014522. 2009. . DOI: 10.1103/PhysRevB.79.014522.

[13] R. W. Gomez, V. Marquina, J. L. Perez-Mazariego, R. Escamilla, R. Escudero, M. Quintana, J. J. Hernandez-Gomez, R. Ridaura and M. L. Marquina. Effects of substituting se with te in the FeSe compound: Structural, magnetization and mossbauer studies. *JOURNAL OF SUPERCONDUCTIVITY AND NOVEL MAGNETISM} 23}(4)},* pp. 551-557}. 2010}. . DOI: {10.1007/s10948-010-0764-2.

[14] Y. Mizuguchi, F. Tomioka, S. Tsuda, T. Yamaguchi and Y. Takano. Substitution effects on FeSe superconductor. *JOURNAL OF THE PHYSICAL SOCIETY OF JAPAN} 78}(7}),* 2009}. . DOI: {10.1143/JPSJ.78.074712.

[15] K. Yeh, T. Huang, Y. Huang, T. Chen, F. Hsu, P. M. Wu, Y. Lee, Y. Chu, C. Chen, J. Luo, D. Yan and M. Wu. Tellurium substitution effect on superconductivity of the Î±-phase iron selenide. *EPL (Europhysics Letters) 84(3),* pp. 37002. 2008. Available: http://stacks.iop.org/0295-5075/84/i=3/a=37002.

[16] A. S. Sefat. Bulk synthesis of iron-based superconductors. *CURRENT OPINION IN SOLID STATE \& MATERIALS SCIENCE} 17}(2}),* pp. 59-64}. 2013}. . DOI: {10.1016/j.cossms.2013.04.001.

[17] Y. Xia, F. Huang, X. Xie and M. Jiang. Preparation and superconductivity of stoichiometric beta-FeSe. *Epl 86(3),* pp. 37008. 2009. . DOI: 10.1209/0295-5075/86/37008.

[18] X. Li, Z. Gao, Y. Liu, Z. Ma and L. Yu. Influence of premilling time on the sintering process and superconductive properties of FeSe. *IEEE Trans. Appl. Supercond. 22(6),* pp. 7300105. 2012. . DOI: 10.1109/TASC.2012.2219048.

[19] X. Li, Z. Ma, Y. Liu, M. Dong and L. Yu. The sintering process and superconductivity of polycrystalline milled fe-se. *IEEE Trans. Appl. Supercond. 23(2),* pp. 7000405. 2013. . DOI: 10.1109/TASC.2013.2246159.

[20] X. Li, Z. Gao, Y. Liu, Z. Ma, L. Yu, H. Li and H. Yang. The microstructures and superconducting properties of FeSe0.5Te0.5 bulks with original milled powders. *Cryogenics 57(0),* pp. 50. 2013. Available: http://www.sciencedirect.com/science/article/pii/S0011227513000477. DOI: http://dx.doi.org/10.1016/j.cryogenics.2013.05.003".

[21] H. Rietveld. A profile refinement method for nuclear and magnetic structures. *Journal of Applied Crystallography 2(2),* pp. 65. 1969. . DOI: 10.1107/S0021889869006558.

[22] Z. Gao, Y. Qi, L. Wang, D. Wang, X. Zhang, C. Yao and Y. Ma. Superconducting properties of FeSe wires and tapes prepared by a gas diffusion technique. *Supercond. Sci. Technol. 24(6),* pp. 065022. 2011. . DOI: 10.1088/0953-2048/24/6/065022.

[23] Y. Mizuguchi, H. Izawa, T. Ozaki, Y. Takano and O. Miura. Transport properties of single- and three-core FeSe wires fabricated by a novel chemical-transformation PIT process. *Supercond. Sci. Technol. 24(12),* pp. 125003. 2011. . DOI: 10.1088/0953-2048/24/12/125003.

[24] T. Ozaki, K. Deguchi, Y. Mizuguchi, Y. Kawasaki, T. Tanaka, T. Yamaguchi, H. Kumakura and Y. Takano. Fabrication of binary FeSe superconducting wires by diffusion process. *J. Appl. Phys. 111(11),* pp. 112620. 2012. . DOI: 10.1063/1.4726243.

[25] S. I. Vedeneev, B. A. Piot, D. K. Maude and A. V. Sadakov. Temperature dependence of the upper critical field of FeSe single crystals. *Physical Review B 87(13),* pp. 134512. 2013. . DOI: 10.1103/PhysRevB.87.134512.

[26] H. Lei, R. Hu and C. Petrovic. Critical fields, thermally activated transport, and critical current density of beta-FeSe single crystals. *Physical Review B 84(1),* pp. 014520. 2011. . DOI: 10.1103/PhysRevB.84.014520.

[27] N. Werthamer, E. Helfand and P. Hohenberg. Temperature and purity dependence of superconducting critical field, H_{c2}. III. electron spin and spin-orbit effects. *Physical Review 147(1),* pp. 295. 1966. . DOI: 10.1103/PhysRev.147.295.

[28] S. Margadonna, Y. Takabayashi, M. T. McDonald, K. Kasperkiewicz, Y. Mizuguchi, Y. Takano, A. N. Fitch, E. Suard and K. Prassides. Crystal structure of the new FeSe(1-x) superconductor. *CHEMICAL COMMUNICATIONS} (43}),* pp. 5607-5609}. 2008}. . DOI: {10.1039/b813076k.

[29] M. H. Fang, H. M. Pham, B. Qian, T. J. Liu, E. K. Vehstedt, Y. Liu, L. Spinu and Z. Q. Mao. Superconductivity close to magnetic instability in fe(Se1-xTex)(0.82). *PHYSICAL REVIEW B} 78}(22}),* 2008}. . DOI: {10.1103/PhysRevB.78.224503.